ACS APPLIED MATERIALS & INTERFACES

Research Article

www.acsami.org

Enhanced Field Emission from Reduced Graphene Oxide Polymer Composites

Georgios M. Viskadouros,[†,‡] Minas M. Stylianakis,[†,§] Emmanuel Kymakis,[†,*] and Emmanuel Stratakis*[,†,⊥,#]

[†]Center of Materials Technology and Photonics & Electrical Engineering Department, Technological Educational Institute (TEI) of Crete, Heraklion 71004 Crete, Greece

[‡]Department of Mineral Resources Engineering, Technical University of Crete, Chania, 731 00, Crete, Greece

[§]Department of Chemistry, University of Crete, P.O. Box 2208, 710 03 Heraklion Crete, Greece

[⊥]Institute of Electronic Structure and Laser, Foundation for Research and Technology - Hellas, P.O. Box 1527, 711 10 Heraklion Crete, Greece

[#]Department of Materials Science and Technology, University of Crete, Heraklion, 710 03 Crete, Greece

ABSTRACT: Results on electron field emission (FE) from reduced graphene oxide (rGO):poly(3-hexylthiophene) (P3HT) composite layers are presented. Three different FE cathodes were tested and compared: rGO layers on (a) n^+-Si, (b) composite films with different rGO:P3HT ratios, (c) rGO layers on composite films with different rGO:P3HT ratios. Experiments show that there is a critical rGO:P3HT ratio in which the field-emission performance is remarkably improved. Notably, such performance is always superior to that of the optimum rGO/n^+-Si cathode. On the contrary, it is inferior to that attained upon deposition of a second rGO layer on top of the rGO:P3HT composite showed the best FE performance that showed turn-on field of as low as ~0.9 V/μm and field enhancement factor of ~1900. The contributions of the composite film morphology as well as the role of rGO sheet−substrate interaction on the emission performance are evaluated and discussed.

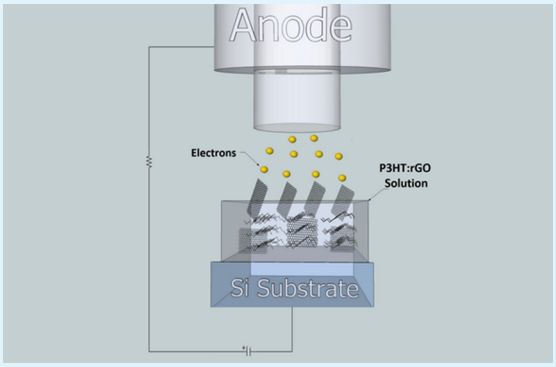

KEYWORDS: *graphene, reduced graphene oxide, field emission, polymer composites, solution-processed*

1. INTRODUCTION

Field-electron emission, otherwise known as cold cathode emission, is a form of quantum mechanical tunneling in which electrons pass through a barrier in the presence of an electric field. This phenomenon is highly dependent on both the properties of the material and the shape of the particular cathode, so that higher aspect ratios (height/tip radius) produce higher field-emission currents at lower applied electric fields. Arrays of conductive or semiconductive structures can be integrated into a large number of devices that utilize cold emission and ballistic transport of electrons from emitting cathodes to appropriate collector electrodes. Accordingly, in the past few years, an intensive research effort has been devoted to design and fabrication of cold cathode electron emitters. Potential applications include vacuum microelectronic devices, such as electron guns and microwave power amplifiers, and FE-based electronic devices, such as flat panel FE displays (FEDs).[1−3]

Because of its inherent 2D geometry, graphene offers a facile material to make large-area field-emission devices.[4] The high aspect ratio of graphene flakes together with the presence of subnanometer edges may render graphene superior field emitter, allowing the extraction of electrons at low threshold electric fields with high geometric field enhancement. Chemical treatment of bulk graphite using strong oxidizing agent (Hummers method) is quite useful for the large scale synthesis of graphene flakes, though in the form of graphene oxide (GO).[5,6] GO shares the similar single and few atomic layer structure of carbon as monolayer or few-layer graphene, respectively, but unlike graphene, the presence of hydroxide and epoxy groups in its lattice makes it highly electrical resistive. This property is undesirable for most of electronic applications and several methods have been proposed in order to reduce GO to rGO, thus improving its conductivity. Among reduction methods commonly applied include the use of chemical reducing agents,[7,8] high-temperature thermal annealing,[9] electric[10,11] and electromagnetic field.[12] Despite its inferior, compared to graphene, conductivity rGO is solution-processable and thus can be deposited in large areas onto any type substrate enabling simple and cost-effective fabrication of field electron emitters for display applications.

Received: October 9, 2013
Accepted: December 9, 2013
Published: December 9, 2013

Table 1. Field-Emission Properties of rGO Layers with Different Sheet Concentrations, Defined in the Text[a]

rGO content (vol %)	20	30	40	50	70
turn-on field F_{to} (V/μm)	4.7 ± 0.1	3.2 ± 0.1	3.6 ± 0.1	4.1 ± 0.1	4.4 ± 0.1
field enhancement β	177	227	203	194	180

[a]The ± values denote the standard deviation of each measured or estimated quantity.

Besides this, in the search for promising new materials for stable and low-threshold field emission cathodes, composites of semiconducting polymers with carbon nanomaterials have recently received considerable attention.[13] This is partly due to the low electron affinity, wide bandgap and excellent transport properties of some conductive organic polymers. More importantly, the flexibility of such polymer-based cathodes can serve toward realization of flexible field emission displays. Finally, a conducting polymer composite can be used as an intermediate host matrix between the partially embedded nanoemitters and a conducting substrate in order to improve the electrical contact, i.e., reduce the contact resistance between the two.[14,15]

In the present contribution, we report on a comparative study of the field emission characteristics of composite rGO:P3HT polymeric cathodes as well as rGO flakes deposited onto various conductive substrates including n^+Si and rGO:P3HT composite layers. The rGO:P3HT ratio was varied to control the structural and electrical properties of the cathodes and polymeric substrates and as a result the FE performance and stability. The deposition method is based on solution casting that is fast and does not require complex equipment. The results indicate that the field-emission stability of composite structures is superior to that of pristine rGO cathodes. Our results show that polymer−rGO composites with the rGO flakes exposed to vacuum may be a promising solution for superior graphene FE cathodes.

2. EXPERIMENTAL SECTION

2.1. Preparation of the Starting GO Solution. GO was prepared from purified natural graphite powder (Alfa Aesar, ~200 mesh) according to a modified Hummers' method.[16,17] A colloidal suspension of individual graphene oxide platelets in purified water (3 mg/mL) was prepared by sonication of GO in an ultrasound bath (Elma S 30 H Elmasonic) for 3 h. Finally, the dispersion was centrifuged for 5 min at 4200 rpm and the green-brown supernatant was separated into a clean vial, whereas the slurry sediment was removed.

2.2. Reduction of Graphene Oxide (GO). Reduction of electrically insulating GO is one of the most promising ways to produce electrically conducting graphene-based flakes on a large scale. In this work, the hydrazine vapor reduction method is used for the realization of the starting rGO solution.[8] GO powder (0.5 g) was placed in a perfectly cleaned glass Petri dish inside a larger glass Petri dish which also contained 0.5 mL of hydrazine monohydrate 98% (Alfa Aesar, Ward Hill, MA). The larger dish was covered with a glass lid, sealed with Parafilm tape, and placed over a hot plate at 40 °C for 18 h, after which the dish was opened and the powder was rinsed with purified water and dried both under an inert atmosphere and by heating to 40 °C in a vacuum. The first indication that the reduction process has taken place to the material is the change of the color after the hydrazine vapor treatment, from yellowish-brown to metallic gray.

2.3. Preparation of rGO-P3HT Solution. ITo prepare homogeneous composite solutions of rGO:P3HT, we individually dissolved each material in tetrahydrofuran (THF), according to the following procedure. Poly(3-hexylthiophene) (P3HT) was dissolved in THF, by magnetic stirring, in a 10 mg/mL concentration. Concurrently, rGO was dispersed in different concentrations in the same solvent by ultrasonication, to form homogeneous colloids. The reduction of rGO, by hydrazine is partially achieved and presents acid groups on its surface.[18−20] Therefore, the polar nature of rGO is not entirely eliminated and thus rGO forms very stable, homogeneous dispersions in THF. Thereafter, rGO colloids were added to the P3HT solutions in controlled volume ratio and sonicated for another 1.5 h to form homogeneous P3HT/rGO composite dispersions. After filtration with cotton to remove the trace amount of precipitate, three different cathode substrates were prepared: (a) Dense and sparse rGO layers were drop-casted on n^+-Si by letting the tetrahydrofuran to evaporate at room temperature. The density of a layer was defined to be equal to the volume fraction of rGO in the initial solution. (b) Composite films with different rGO:P3HT volume ratios were drop casted on n^+-Si. For these composites the corresponding rGO loadings defined as the volume ratio [rGO /(rGO + P3HT)] were 10, 20, 30, 60, and 100%, respectively. (c) rGO layers were drop-casted on previously drop-casted rGO−P3HT composites in various ratios on n^+-Si and were left to dry at room temperature. The surface morphology of the film was examined by field emission scanning electron microscopy (FESEM JEOL-JSM7000F) both before and after field emission. There was no apparent explosive destruction to the film which can be associated with discharge current phenomenon. Results on the average protruding bundle height were determined statistically from these images.

2.4. Field-Emission Measurements. Field emission measurements were performed under high vacuum conditions ($<1 \times 10^{-6}$ Torr), using the samples as cold cathode emitters in a short - circuit protected planar diode system. Details for the experimental setup can be found elsewhere.[21] Current − voltage ($J-U$) curves were taken at the distance between anode−cathode was controlled by a stepper motor and found that field-emission characteristics are not influenced by the anode location. All measurements presented here were performed at t = 200 μm. Several emission cycles were taken in order to verify the stability and the reproducibility of the $J-U$ curves. A voltage with variable sweep step, supplied by a HV source (PS350-SRS), was applied between the anode and the cathode to extract electrons. The emission current was measured using an autoarranging digital Pico-ammeter (Keithley 485) protected against high voltage surges by a MOSFET limiter. The stability of the emission current over time was examined by monitoring the evolution of the emitted current density over a long time period of continuous operation.

3. RESULTS AND DISCUSSION

We have observed that the field-emission performance of pure rGO layers depend on the density of the flakes in the initial solution. We first studied this influence by measuring the field emission $I-U$ characteristics of films prepared via drop casting from solutions of different rGO concentrations. The purpose was to find the critical rGO density for optimum emission and use this particular density for films grown on composite films. Table 1 summarizes the turn-on field, F_{to}, defined as the average macroscopic field needed to extract 25 pA/cm^2, for rGO layers of different density. All films were prepared and deposited under identical conditions. The results in Table 1 show that the best field emitters are the films with medium rGO sheet densities. Both the number and the height of emitters are decreased for low-density films and as a result these are inefficient cathodes. On the other hand, screening effects become significant on very dense films[21,22] and the emission performance degrades again.

Figure 1a shows, on a log−log plot, the current density, J, measured as a function of the bias voltage, U for composite

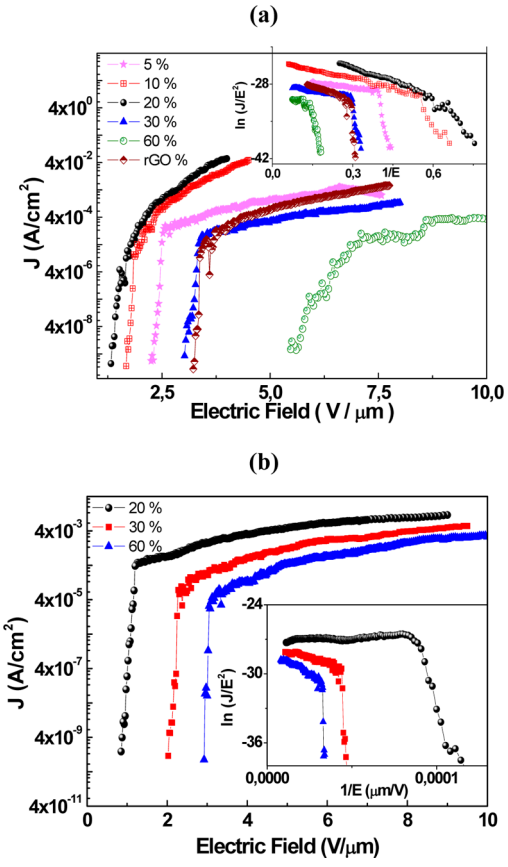

Figure 1. Logarithmic plot of current density–field (J–E) emission characteristics of: (a) rGO:P3HT composite layers with different sheet loadings, shown in the legend and defined in the text and Table 2. The J–E characteristic of a 30 vol % rGO layer deposited on n^+ Si is also shown for comparison. Inset: Fowler–Nordheim plot of the corresponding J–E curves; (b) a 30 vol % rGO layer deposited on rGO:P3HT composite substrates with different sheet loadings, shown in the legend and defined in the text and Table 3. Inset: Fowler–Nordheim plot of the corresponding J–E curves.

layers of different rGO:P3HT ratios. The corresponding F_{to} values are shown in Table 2. Three distinct regions are always visible in the J–U data: zero emission, field emission, and current saturation. Remarkably, the field-emission performance can be improved, at a certain rGO:P3HT ratio. As a general trend, the rGO loading improves emission up until a point after which the emission worsens, possibly due to screening effects. The respective J–U curves for rGO layers casted on composite substrates of different rGO:P3HT ratios are shown in Figure 1b. Remarkably, as shown in Table 3, the FE performance can be further improved when the rGO layer is deposited on top of polymer: rGO composite, with respect to the same layer on n^+ Si substrate.

Figure 2 shows representative top and side-view (45°) FESEM images of the pure rGO sample with the optimum flake

Table 3. FE Properties (turn on field, field enhancement) of rGO:P3HT Composites with Different Graphene Contents with an Extra rGO Layer[a]

rGO/(rGO +P3HT) ratio (vol %)	20	30	60
turn-on field F_{to} (V/μm)	0.9 ± 0.1	2.2 ± 0.1	2.9 ± 0.1
edge density (cm^{-2})	3200	630	480
field enhancement β	1900	395	342

[a]The ± values denote the standard deviation of each measured or estimated quantity.

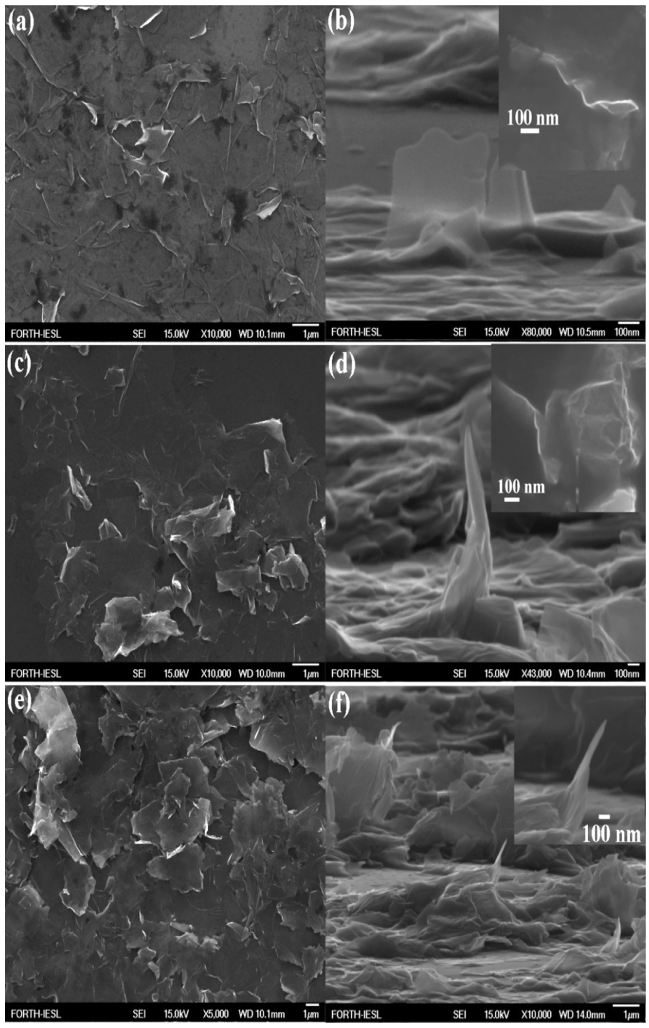

Figure 2. Top (left) and 45° (right) FESEM views displaying: (a, b) a pure rGO layer on n^+Si; (c, d) a 20% rGO:P3HT layer on n^+Si; (e, f) rGO layer onto an 20% rGO:P3HT substrate. The insets present high-magnification image of sharp graphene edges (b, d) as well as graphene–polymer bundles.

density deposited on Si (Figure 2a, b), the composite structure on Si with the best FE performance (Figure 2c, d), and an rGO layer on top of the best emitting composite substrate (Figure

Table 2. FE Properties of rGO-P3HT Composites with Different Graphene Contents without the Extra rGO Layer[a]

rGO/(rGO +P3HT) content ratio (vol %)	5	10	20	30	60	100
turn-on field F_{to} (V/μm)	2.4 ± 0.1	1.7 ± 0.1	1.2 ± 0.1	3.0 ± 0.1	5.5 ± 0.1	3.2 ± 0.1
edge density (cm^{-2})	480	1010	2450	500	110	390
field enhancement β	283	831	1529	279	145	227

[a]The ± values denote the standard deviation of each measured or estimated quantity.

dx.doi.org/10.1021/am4044618 | ACS Appl. Mater. Interfaces 2014, 6, 388–393

2e, f). Top-view images show that in all cases the rGO flakes were uniformly laid flat onto the substrate while the sheets comprise sharp edges protruding out of the surface. In the composite films, the number density of sharp edges, N, increases, whereas some rGO sheets are entangled with the polymer chains. Indeed, as shown in Table 2, a characteristic increase in N is observed for low rGO content, whereas it decreases as the polymer content becomes high. Furthermore, the surface profile formed by the rGO sheets becomes rough at low rGO contents, indicating orientation of the sheets at different angles with respect to the planar substrate (Figure 2c). On the contrary for high polymer contents fewer rGO sheets are exposed to vacuum (not shown). Finally, as shown in Table 3, N always increases when rGO layer is deposited onto composite films. This may also be related to the observation that the layer roughness of the top rGO layer also increases (Figure 2e). Side-view FESEM images show that many rGO sheets and bundles with edge diameter of less than 10 nm were protruding from the bulk (insets of Figure 2d, f). It should also be noted that in samples with high rGO concentration, the base of the protruding bundles is a part of the rGO layer, whereas in the case of samples with high polymer content, bundles are sticking out of a polymer bulk. This observation suggests that there are two conduction processes present, conduction between rGO within flakes a bundle and between polymer and sheets.[23] Both processes are vital for analyzing the field-emission performance of the composites. We analyze our field emission data within the frame of a Fowler–Nordheim (FN) field-assisted tunneling process[24] in which the current density, J, depends on the local microscopic field at the emitter, F_{loc}, according to the relationship

$$J = AF_{loc}^2 \exp\left(-\frac{b_{FN}}{F_{loc}}\right) \quad (1)$$

where A is a constant that depends on the actual emitting surface structure $b_{FN} = 0.94B\Phi^{3/2}$ with $B = 6.83 \times 10^7$ V cm^{-1}eV$^{-3/2}$, and Φ is the work function of the material in eV. F_{loc} is usually related to the average macroscopic field, F, as follows

$$F_{loc} = \beta F = \beta \frac{U}{t} \quad (2)$$

where β is the field enhancement factor, U is the applied voltage, and t is the sample–anode distance.

The insets in panels a and b in Figure 1 show the FN plots of the corresponding J–U curves. The field-enhancement factors are determined by fitting the linear part of the data at low voltages, following eq 1, assuming a work function Φ of 5.0 eV for rGO.[25] The corresponding dependence of the turn-on field, F_{to}, as well as of β on the rGO/P3HT ratio is shown in Figure 3. Indeed, the best emission properties are achieved when the rGO/P3HT ratio of the composite substrate is 1:4. Accordingly, an increase in the F_{to} is observed in the case of substrates with high polymer concentration. When the rGO solution was put on top of the polymer, the solvent of the rGO solution dissolves some of the polymer on the surface, causing a part of the rGO flakes and/or bundles to be buried inside the polymer. Consequently, as the rGO/P3HT ratio decreases, i.e the polymer content increases, the rGO density into the polymer matrix decreases giving rise to a corresponding decrease in the density of the rGO edges exposed to vacuum. Besides this, when the polymer content is very low, rGO sheets

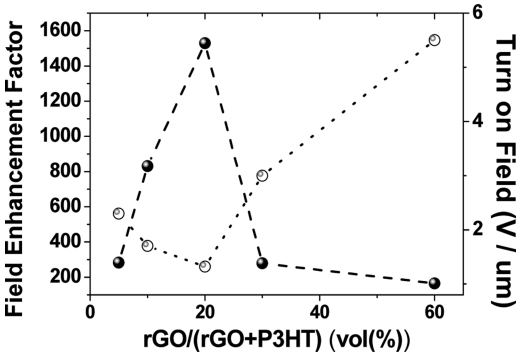

Figure 3. Variation of the turn on field (dotted line) and the enhancement factor (dashed line) for different compositions of the rGO:P3HT layer.

become more preferentially oriented parallel to the substrate and less emitting edges are exposed to vacuum; as a result the emission performance falls again. The experimental evidence that supports this argument is given by the average density of sharp edges determined from FESEM images (Table 2), where it is shown that it becomes lower for samples with substrates of high and very low polymer contents. It therefore seems that the number of active emitters changes with polymer loading and becomes optimum at a critical composite concentration.

An additional field-enhancement source has been proposed on the basis of the existence of a triple junction between the, semimetal, rGO, the semiconducting matrix P3HT and vacuum.[26] In a triple junction, the surface potential undergoes a step change at the junction between the rGO and the polymer due to the difference in work function between the two materials. This surface potential irregularity will modify the potential lines immediately above the two materials in vacuum, in the vicinity of the junction. In this regard, it is possible to explain the electron emission mechanism for rGO:P3HT composites as follows: emission of the electrons from the surface at the rGO sheet/polymer/vacuum triple junction occurs due to an enhancement of the applied field brought about by the aspect ratio of the sharp edge, each of which will have a thin polymer coating.

Current saturation at high fields and thus the appearance of a knee point in F–N plots can be attributed to either resistive heating or high contact resistance effects. A similar saturation effect was observed in CNT films and attributed to adsorbents on the emitter tip[27] and a large voltage drop along the emitter and/or at the emitter/substrate interface.[28,29]

Another important parameter that is crucial for device applications is the stability of the FE current over time. Panels a and b in Figure 4 present the evolution of the emission current density at a constant bias voltage of 1800 V over a long period of continuous operation for rGO on n$^+$Si and the best emitting rGO on rGO:P3HT cathode, respectively. It can be observed that the emission current lasts for about 40 h in the case of the rGO/n$^+$Si and ~60 h for the rGO/rGO:P3HT cathodes. The fluctuations of the emission current observed are commonly attributed to molecular adsorption on and/or ion bombardment of the emitting sites by residual gases, both of which are favored under high-vacuum conditions for graphitic based emitters.[30] However, resistive heating of the nanotube core and emitting apex have been experimentally observed and thought as the main reason of emission degradation.[31,32] For the composite film the situation can be improved, provided that the

dx.doi.org/10.1021/am4044618 | ACS Appl. Mater. Interfaces 2014, 6, 388–393

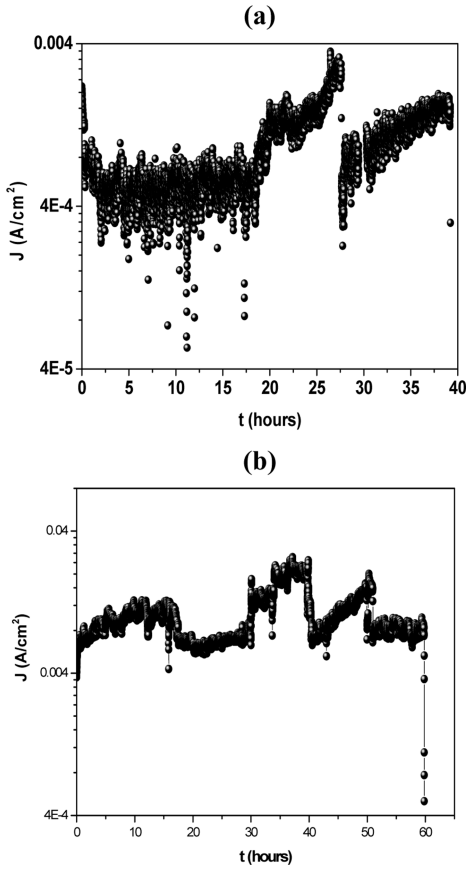

Figure 4. Emission current stability over time at a constant voltage bias, for (a) an rGO layer on n^+ Si, (b) the same rGO layer deposited on the 20% composite rGO:P3HT substrate.

rGo sheets or parts of them are covered with polymer as it is indeed observed to take place for samples with a polymer content, at the FESEM images (Figure 2). Heat conduction during emission can thus be facilitated through the polymer bulk diverging from the case of bare sheets where heat is only conducted through the sheets themselves. Heat dissipation is expected to be more effective in the case of the composite films as the thermal conductivity of the polymer matrix is 100 mW/mK,[33] i.e., four times higher than that of air at ambient conditions. Because the bare rGO sheets operate in vacuum, the discrepancy between the two conductivities will be much higher, rendering the polymer matrix an efficient heat sink for the rGO emitters. Such a mechanism may protect the emission sites from degradation and increase the cathode lifetime.

Finally, Table 4 depicts comparison of the turn-on field values and the enhancement factor reported for carbon based allotropes/mixed systems. In this way, a direct comparison of the performance of each system takes place.

4. CONCLUSIONS

In this report, we have compared the field-emission characteristics among rGO composites with a conjugated polymer. It is found that the performance of the optimized composite cathode is always superior to that of the optimum rGO/n^+-Si cathode. More importantly, it is found that the field-emission stability of composite rGO layer is superior to that of pure rGO cathode, probably because of better heat conduction, compared to the optimum pristine rGO film. The experimental results presented here reveal that good rGO field emitters can be produced in a simple process without the need for any sophisticated equipment. Our work may open the way for the potential use of polymer:rGO composites for applications related to flexible field-emission displays.

Table 4. Comparative Table of the Field-Emission Characteristics of Recently Reported Carbon-Based Allotropes/Mixed Systems

type of carbon field emitter	field enhancement factor (β)	turn-on field (V/μm)	ref
rGO polymer composites on Si substrate	1900	0.9	this work
graphene films by electrophoretic deposition on ITO substrate	3700	2.3	34
graphene composites on Si substrate	1200	4	13
chemical-reduced graphene oxide (rGO) on titanium (Ti)-coated silicon substrates		3	35
few-layer graphene on silicon substrate	3000	1	36
hydrogen exfoliated grapheme on flexible carbon cloth	4907	1.18	37
screen-printed grapheme on silicon substrate	4539	1.5	38
vertical few layer grapheme on silicon substrate	6795	1.8	39
plasma treatment of vertically aligned few-layer grapheme on Si substrate	5130	2.23	40
free-standing graphene on microstructured silicon vertices	1604	2.3	14
single-layer graphene on Si substrate	1656	50	41
graphene on PET substrate	1000	1.75	42
graphite nanoplatelet (GNP) on Si substrate	2135	4.47	43
vertical graphite sheets on graphite-encapsulated Cu	6450	2.4	44
acid-oxidized multiwall carbon nanotubes deposited on paper substrates	4740	0.8	45
amorphous CNT functionalized with CuPc	1970.4	3.05	3
CNT/TEOS on SWNT/PET films	5607	1.76	46
vertically aligned carbon nanotube mesh,on glass substrate	2400	5	47
vertically aligned carbon nanotubes onto Ni-coated highly polished graphite substrates	1200	2	48
vertically aligned carbon nanotubes on plastic substrates	6222	1.13	49
carbon nanowalls on forests of conical Si microspikes	3533	0.9	2
horizontally aligned CNT	3500	2.2	50
MWCNTs decorated with nanoscale metal clusters	1292	2.10	51

AUTHOR INFORMATION

Corresponding Authors

*E-mail: kymakis@staff.teicrete.gr. Tel: 2810-379895.
*E-mail: stratak@iesl.forth.gr. Tel: 2810-391274.

Notes

The authors declare no competing financial interest.

ACKNOWLEDGMENTS

This research has been cofinanced by the European Union (European Social Fund—ESF) and Greek national funds through the Operational Program "Education and Lifelong Learning" of the National Strategic Reference Framework (NSRF)-Research Funding Program: ARCHIMEDES III

Investing in knowledge society through the European Social Fund.

REFERENCES

(1) Engelsen, D. E. *Phys. Proc.* **2008**, *1*, 355−365.
(2) Stratakis, E.; Giorgi, R.; Barberoglou, M.; Dikonimos, Th.; Salernitano, E.; Lisi, N.; Kymakis, E. *Appl. Phys. Lett.* **2010**, *96* (4), No. 043110.
(3) Jha, A.; Ghorai, U. K.; Banerjee, D.; Mukherjee, S.; Chattopadhyay, K. K. *RSC Adv.* **2013**, *3*, 1227−1234.
(4) Lahiri, I.; Verma, V. P.; Choi, W. *Carbon* **2011**, *49*, 1614−1619.
(5) An, X.; Liu, F.; Jung, Y. J.; Kar, S. *J. Phys. Chem. C* **2012**, *116*, 16412−16420.
(6) Dikin, D. A; Stankovich, S.; Zimney, E. J; Piner, R. D; Geoffrey, H.; Dommett, B.; Evmenenko, G.; Nguyen, S. T; Ruoff, R. S. *Nature* **2007**, *448*, 457−460.
(7) Wakeland, S.; Martinez, R.; Grey, J. K; Luhrs, C. C. *Carbon* **2010**, *48*, 3463−3470.
(8) Sungjin, P.; Jinho, A.; Potts, J. R.; Velamakanni, A.; Murali, S.; Ruoff, R. S. *Carbon* **2011**, *49*, 3019−3023.
(9) Akhavan, O. *Carbon* **2010**, *48*, 509−519.
(10) Sahoo, S.; Khurana, G.; Barik, S. K.; Dussan, S.; Barrionuevo, D.; Katiyar, R. S. *J. Phys. Chem. C* **2013**, *117*, 5485−5491.
(11) Guo, Y.; Wu, B.; Liu, H.; Ma, Y.; Yang, Y.; Zheng, J.; Yu, G.; Liu, Y. *Adv. Mater.* **2011**, *23*, 4626−4630.
(12) Wu, Z. S.; Pei, S.; Ren, W.; Tang, D.; Gao, L.; Liu, B.; Li, F.; Liu, C.; Cheng, H. M. *Adv. Mater.* **2009**, *21*, 1756−1760.
(13) Eda, G.; Unalan, H. E.; Rupesinghe, N.; Amaratunga, G. A. J.; Chhowalla, M. *Appl. Phys. Lett.* **2008**, *93*, 233502.
(14) Stratakis, E.; Eda, G.; Yamaguchi, H.; Kymakis, E.; Fotakis, C.; Chhowalla, M. *Nanoscale* **2012**, *4*, 3069−3074.
(15) Latham, R. V. *High Voltage Vacuum Insulation: The Physical Basis*; Academic Press: London, 1981.
(16) Stylianakis, M. M.; Stratakis, E.; Koudoumas, E.; Kymakis, E.; Anastasiadis, S. H. *ACS Appl. Mater. Interfaces* **2012**, *4*, 4864−4870.
(17) Luo, Z.; Lu, Y.; Somers, L. A.; Johnson, A. T. C. J. *Am. Chem. Soc.* **2009**, *131*, 898−899.
(18) Park, S.; Ruoff, R. S. *Nat. Nanotechnol.* **2009**, *4*, 217−224.
(19) Dreyer, D. R.; Park, S.; Bielawski, C. W.; Ruoff, R. S. *Chem. Soc. Rev.* **2010**, *39*, 228−240.
(20) Verdejo, R.; Mar Bernal, M.; Romasanta, L. J.; Lopez-Manchado, M. A. *J. Mater. Chem.* **2011**, *21*, 3301−3310.
(21) Zorba, V.; Tzanetakis, P.; Fotakis, C.; Spanakis, E.; Stratakis, E.; Papazoglou, D. G; Zergioti, I. *Appl. Phys. Lett.* **2006**, *88*, 081103.
(22) Nillson, L.; Groening, O.; Emmenegger, C.; Kuettel, O.; Schaller, E.; Schlapbach, L.; Kind, H.; Bonard, J. M.; Kern, K. *Appl. Phys. Lett.* **2000**, *76*, 2071.
(23) Kymakis, E.; Amaratunga, G. A. J. *J. Appl. Phys.* **2006**, *99*, 084302.
(24) Modinos, A. *Field, Thermionic, And Secondary Electron Emission Spectroscopy*; Plenum Press, New York, 1984.
(25) Ivey, H. F. *Phys. Rev.* **1949**, *76*, 567.
(26) Alexandrou, I.; Kymakis, E.; Amaratunga, G. A. J. *Appl. Phys. Lett.* **2002**, *80*, 1435.
(27) Chuang, A. T. H.; Robertson, J.; Boskovic, B. O.; Koziol, K. K. K. *Appl. Phys. Lett.*. **2007**, *90*, 123107.
(28) Minoux, E.; Groening, O.; Teo, K. B. K.; Dalal, S. H.; Gangloff, L.; Schnell, J. P.; Hudanski, L.; Bu, I.Y. Y.; Vincent, P.; Legagneux, P.; Amaratunga, G. A. J.; Milne, W. I. *Nano Lett.* **2005**, *5*, 2135.
(29) Zhao, W. J.; Rochanachivapar, W.; Takai, M. J. *Vac. Sci. Technol., B* **2004**, 1834−1837.
(30) Min, Q. M.; Feng, T.; Ding, H.; Lin, L.; Li, H.; Chen, Y.; Sun, Z. *Nanotechnology* **2009**, *20*, 425702.
(31) Kayastha, V. K.; Ulmen, B.; Yap, Y. K. *Nanotechnology* **2007**, *18*, 035206.
(32) Purcell, S . T.; Vincent, P.; Journet, C.; Binh, V. T. *Phys. Rev. Lett.* **2002**, *88*, 105502−1.
(33) Thompson, E. V. *Encyclopedia of Polymer Science and Engineering*; John Wiley & Sons: New York, 1989; Vol. *16*, pp711−747.
(34) Zhong-Shuai, W.; Songfeng, P.; Wencai, R.; Daiming, T.; Libo, G.; Bilu, L.; Feng, L.; Chang, L.; Hui-Ming, C. *Adv. Mater.* **2009**, *21* (17), 1756−1760.
(35) Jun, L.; Chen, J.; Luo, B.; Yan, X.; Xue, Q. *AIP Adv. 2* **2012**, 022101.
(36) Malesevic, A.; Kemps, R.; Vanhulsel, A.; Chowdhury, M. P.; Volodin, A.; Haesendonck, C. V. *J. Appl. Phys.* **2008**, *104*, 084301.
(37) Baby, T. T.; Ramaprabhu, S. *Appl. Phys. Lett.* **2011**, *98*, 183111.
(38) Qian, M.; Feng, T.; Ding, H.; Lin, L.; Li, H.; Chen, Y.; Sun, Z. *Nanotechnology* **2009**, *20*, 425702.
(39) Zhang, Y.; Du, J.; Tang, S.; Liu, P.; Deng, S.; Chen, J.; Xu, N. *Nanotechnology* **2012**, *23*, 015202.
(40) Qi, J. L.; Wang, X.; Zheng, W. T.; Tian, H. W.; Hu, C. Q.; Peng, Y. S. *J. Phys. D: Appl. Phys.* **2010**, *43*, 055302.
(41) Xiao, Z.; She, J.; Deng, S.; Tang, Z.; Li, Z.; Lu, J.; Xu, N. *ACS Nano* **2010**, *4* (11), 6332−6336.
(42) Verma, V. P.; Das, S.; Lahiri, I.; Choi, W. *Appl. Phys. Lett.* **2010**, *96* (20), No. 203108.
(43) Song, Y.; Shin, D. H.; Song, Y. H.; Saito, Y.; Lee, C. H. *Appl. Phys. Lett.* **2013**, 073112.
(44) Wang, S. M.; Tian, H. W.; Meng, Q. N.; Zhao, C. M.; Qiao, L.; Bing, Y. F.; Hu, C. Q.; Zheng, W. T; Liu, Y. C. *Appl. Surf. Sci.* **2012**, *258*, 6930.
(45) Lyth, S. M.; Silva, S. R. P. *Appl. Phys. Lett.* **2007**, *90*, 173124.
(46) Jeong, H. J.; Jeong, H. D.; Kim, H. Y.; Kim, J. S.; Jeong, S. Y.; Han, J. T.; Bang, D. S.; Lee, G. W. *Adv. Funct. Mater.* **2011**, *21* (8), 1526−1532.
(47) Li, C.; Zhang, Y.; Mann, M.; Hasko, D.; Lei, W.; Wang, B.; Chu, D.; Pribat, D.; Amaratunga, G. A. J.; Milne, W. I. *Appl. Phys. Lett.* **2010**, *97* (11), No. 113107.
(48) Chhowalla, M.; Ducati, C.; Rupesinghe, N. L.; Teo, K. B. K.; Amaratunga, G. A. J. *Appl. Phys. Lett.* **2001**, *79* (13), 2079−2081.
(49) Tsai, T. Y.; Lee, C. Y.; Tai, N. H.; Tuan, W. H. *Appl. Phys. Lett.* **2009**, *95* (1), No. 013107.
(50) Jung, S. M.; Jung, H. Y.; Suh, J. S. *Carbon* **2008**, *46*, 1973.
(51) Rakhi, R. B.; Reddy, A. L. M.; Shaijumon, M. M.; Sethupathi, K.; Ramaprabhu, S. J. *Nanopart. Res.* **2008**, *10*, 179.